*Int. J. Solids Structures* Vol. 29, No. 20, pp. 2471–2492, 1992
Printed in Great Britain.

0020-7683/92 $5.00 + .00


# ELASTIC CONTACT VERSUS INDENTATION MODELING OF MULTI-LAYERED MATERIALS

HUAJIAN GAO, CHENG-HSIN CHIU and JIN LEE
Division of Applied Mechanics, Stanford University, Stanford, CA 94305, U.S.A

(*Received* 2 *September* 1991; *in revised form* 11 *February* 1992)

**Abstract**—The elastic contact problem of a rigid cylindrical punch indenting a multi-layered linear elastic half space is studied and then used to model the unloading phase of a microindentation test of thin films deposited on a substrate. First, we adopt a moduli-perturbation method to construct a closed-form, first-order-accurate solution for the contact compliance of a nonhomogeneous medium with a piecewise constant (layered) or continuously varying moduli in the depthwise direction. These solutions are used to estimate the unloading compliance associated with the indentation testing of an Aluminum thin film deposited on a Silicon substrate. Comparison with results obtained from numerical computations indicates that the perturbation estimates are approximately valid for a moderate range of material combinations of practical importance. Also, a finite element analysis is performed to investigate the effects of a penny-shaped debonding crack along the film/substrate interface on the unloading compliance, and to analyse the energy release rate which drives the interface crack. Important conclusions include: (i) interface debonding can cause a significant increase in the unloading compliance of an indentation test; (ii) there exists a saturation crack size beyond which the compliance no longer changes significantly with the crack length; (iii) the plastic deformation near the indenter does not appreciably affect the unloading compliance, but it plays a major role in maintaining the long range energy release rate which drives the crack growth.

## INTRODUCTION

Depth-sensing indentation tests have become widely used in determining mechanical properties of homogeneous and layered materials such as thin films on substrates. This experimental technique has stimulated theoretical modeling which often requires a fundamental understanding of elastic contact problems associated with a nonhomogeneous medium.

Loubet *et al.* (1984) first adopted the elastic solution to a rigid cylindrical punch indenting a homogeneous half space to model the unloading process of a Vickers indenter penetrating into a Magnesium Oxide crystal. In agreement with the elastic solution, they found that the measured unloading compliance $d\tilde{t}/dF$, i.e. the inverse slope of the unloading plot of load $F$ versus total indentation depth $\tilde{t}$, is linearly dependent on the inverse of the plastic penetration depth $1/t_p$ by a material constant $(1-\nu)/\mu$, where $\nu$ and $\mu$ denote, respectively, the Poisson ratio and shear modulus. These authors then suggested that the indentation test could be used as a convenient approach for determining elastic constants. Doerner and Nix (1986) extended this idea to indentation of thin films deposited on substrates. Due to the lack of elastic contact solutions for layered materials, Doerner and Nix (1986) introduced an "effective" contact modulus, $[(1-\nu)/\mu]_{\text{eff}}$, expressed as some linear combination of the modulus of the film and that of the substrate. In that procedure, a fraction coefficient had to be determined by fitting a proposed function to measured experimental data. King (1987) performed an integral equation analysis and modified the formula proposed by Doerner and Nix to fit his numerical results. Subsequently, Shield and Bogy (1989) presented a more thorough treatment for the problem of an axisymmetric rigid cylindrical punch indenting a layered half space by using integral transforms to derive singular integral equations which can be solved numerically via expansion in orthogonal polynomials. Their solution predicts partial separation within the contact region for stiff layers on a relatively soft substrate. However, application of elastic solutions with partially separated contact areas to an indentation test is very questionable because the indenter is expected to be in complete contact with the layered medium after extensive plastic penetration has occurred. Yu *et al.* (1990) also formulated an integral equation approach to study the axisymmetric contact problem involving an elastic layer either in frictionless contact (no adhesion) or perfectly bonded to an elastic half space.

Parallel to the above studies of elastic contact problems, finite element methods (FEM) with fully nonlinear, elastic–plastic analysis capabilities have also been developed to directly simulate an indentation test (e.g. Bhattacharya and Nix, 1988; Laursen and Simo, 1992). Such nonlinear numerical analyses are obviously necessary in order to evaluate the stress distribution and plastic deformation near the indenter region. However, the unloading compliance has been found to be insensitive to the plastic deformation and agree closely with results predicted from elastic contact solution. Based on their finite element simulation of Al/Si thin film system, Laursen and Simo (1992) found that local plastic flow may give rise to pile-up of material near the indenter for soft films on hard substrates and sink-in of material for hard films on soft substrates; the actual contact area between the indenter and the film also varies during the indenter withdrawal. These results significantly enhanced our basic understanding of the plastic deformation involved in the indentation process and provided valuable insights on how the contact area is affected by local plastic flow. For sub-micrometer scale, ultrathin films on substrate, further investigations are needed because inelastic material properties such as yield strength, friction properties as well as the overall constitutive relation will depend very sensitively on the microstructures that exist in thin films and on the dimension of the films themselves.

Our work reported in this paper has been motivated by the above researches and the need to better understand the indentation contact of multi-layered materials. Following previous investigations, the unloading process of a rigid indenter penetrating a thin film on substrate, as schematically shown in Fig. 1(a), will be modeled by a rigid cylindrical punch in frictionless contact with a layered elastic half space, as shown in Fig. 1(b). Our analysis differs from previous studies in a number of aspects. First, we devise a first order rigorous moduli-perturbation method to derive a closed-form solution for the contact compliance of an uncracked film/substrate medium, which has an advantage over previous analyses that are mostly of a numerical analysis nature. The perturbation analysis is based on the

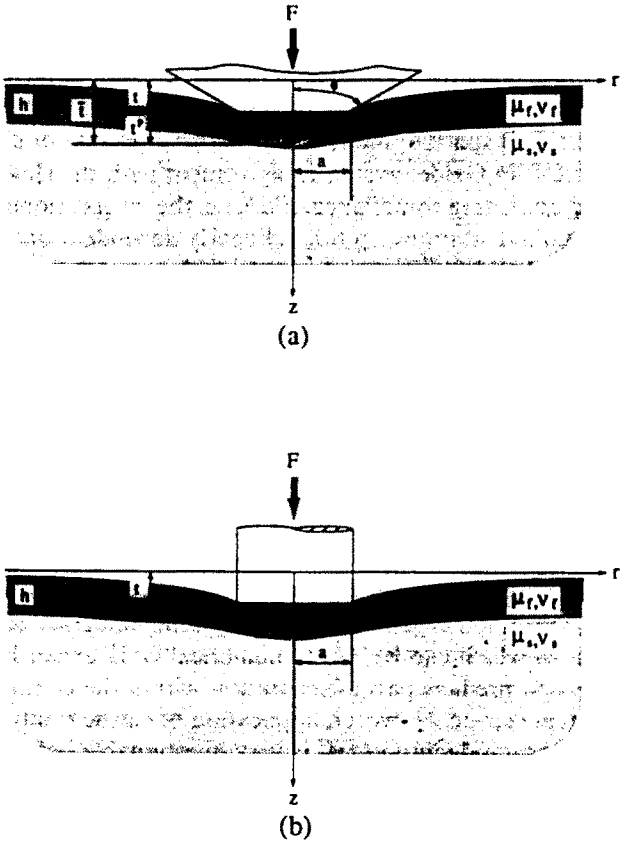


Fig. 1. (a) A conical indenter penetrating a film/substrate medium. (b) A rigid cylindrical punch indenting a layered half space.

known elastic solutions for a reference homogeneous body and the perturbation solution is written in such a form that exact solutions are retained in two limiting cases as the two-phase film/substrate medium approaches a homogeneous body made entirely of the film or the substrate material. Further, we show that the perturbation analysis actually provides a first-order compliance solution to an elastically nonhomogeneous half space with arbitrary, piecewise constant (layered) or continuously varying, elastic moduli in the depthwise direction. Comparison with results obtained from numerical computations indicates that our closed-form perturbation solution is applicable for a moderate range of material combinations of practical importance.

To provide further motivation for this work, we note that, for the indentation contact problem at hand and countless other mechanics problems associated with a multi-layered material system, various numerical approaches, including methods of integral equations, boundary elements and finite elements, are, at least in principle, all capable of providing numerical solutions for given geometrical and material parameters. But a critical issue is whether one will be able to extract the desired information with the least amount of effort and greatest simplicity. Here we wish to show that, by using a moduli perturbation method, it is indeed possible to construct some closed-form simple solutions which agree reasonably well with, but are much simpler to apply than, the results obtained by other numerical methods.

The recent experimental work of Wu *et al.* (1990a) suggested that the interface bonding strength may have a substantial effect on the measured indentation compliance; these authors found that, for two film/substrate specimens of identical material but with different interface adhesion strength, the measured unloading stiffness (or compliance) could differ significantly. Wu *et al.* (1990a) conjectured that interfacial debonding may have occurred in the specimen with weaker interface. Further experiments by Wu and coworkers on indentation fatigue and scratch tests (Wu, 1991; Wu *et al.*, 1990b) also indicated the importance of interfacial debonding in the mechanical failure of a thin film/substrate structure. In response to these findings, we perform an elastic finite element analysis to examine the effects of interfacial debonding on the unloading compliance and the energy release rate which drives the growth of a debonding crack. To simplify the analysis, the effects of plastic deformation generated during indentation are represented by a dilatational transformation strain field in the film in the neighborhood of the indenter. A special scheme of penalty and iteration method is used to treat the interface crack problem, in which the upper and lower crack surface nodes either remain bonded or move independently in the normal direction, depending on the resulting surface tractions along the crack surfaces. To simulate frictionless contact between the crack faces, these crack surface nodes are allowed to slide freely against each other in the horizontal direction. Iteration is used to determine the correct vertical displacements of the crack surface nodes since the crack surface traction and the actual contact area are not known *a priori*. The energy release rate $G$ at the interfacial crack tip, as the driving force for crack growth along the interface, is estimated by the virtual crack extension method in the case of a small crack and by a plane stress plate model for the debonded film in the case of a large crack.

As we will show later in the paper, the FEM analysis reveals that the elastic contact compliance could be increased substantially (up to 25% among the cases we have considered) by cracking along the film/substrate interface. There exists a saturation crack size beyond which the unloading compliance no longer changes significantly with the crack length. By comparing the results with and without the presence of a dilatational inelastic strain, it is verified that the plastic deformation does not appreciably affect the unloading compliance. However, an estimate of the energy release rate shows that the plastic strain provides a dominant driving force for the long range growth of an interface crack.

## FIRST ORDER ELASTIC CONTACT SOLUTIONS FOR AN UNCRACKED LAYERED MEDIUM

### *Geometry and statement of the problem*

In this section, we present a remarkably simple first order perturbation solution for the compliance of a rigid cylindrical punch in frictionless contact with a layered elastic

medium, as shown in Fig. 1(b). The materials are assumed to be isotropic with shear modulus $\mu$ and Poisson's ratio $\nu$. Subscripts f or s will be attached for reference to the properties of the film or the substrate.

Following Doerner and Nix (1986), the problem depicted in Fig. 1(b) will be used to model the unloading process of a conical or pyramidal indenter penetrating into a thin film deposited on substrate, as schematically illustrated in Fig. 1(a). Conceptually, the total indentation depth $\tilde{t}$ can be divided into two parts: the "plastic" depth $t_p$ and the elastic depth $t$. During unloading $t$ is fully recoverable and $t_p$ is assumed to remain constant. In this manner, the unloading process can be approximately modeled as one of elastic contact between a rigid cylindrical punch and the film/substrate material having a circular contact area that is taken to be equal to that of the projected area of the penetration region of the actual indenter (Loubet *et al.*, 1984; Doerner and Nix, 1986). For a conical indenter, the contact radius $a$ and the plastic depth $t_p$ are related by $t_p = a/\tan\phi$ where $\phi$ is the half indenter angle.

The punch model for indentation assumes constant contact area between the indenter and sample during unloading. The finite element simulation of Laursen and Simo (1992) indicated that the actual contact area may change dramatically during the full range of unloading (by as much as 50% for Al/Si). However, for initial unloading the contact area does appear to remain constant [e.g. see Fig. 3.9, Laursen and Simo (1992)]. It is thus appropriate to model the elastic behavior during initial unloading as that of a flat-ended cylindrical punch so that the linear portion of the unloading curve can be used to extract the elastic properties. Nevertheless, one should note that the parameter $t_p$, while instructively called the "plastic depth", may not be equal to the real plastic penetration depth, but rather corresponds to the depth of the contact region when unloading begins. As elastic rebounding proceeds, part of $t_p$ could be recovered and only the residual indentation depth at zero indenting force represents the real plastic penetration. A better elastic contact model incorporating the full nonlinear unloading behavior is certainly desirable. But such models will inevitably result in a great compromise in mathematical simplicity of the analysis.

We shall follow a first order moduli-perturbation method [e.g. Gao (1991)] in which the displacements and stresses in a nonhomogeneous medium are determined based on the known solutions to a reference homogeneous body, as in Fig. 2. For the axisymmetric frictionless punch problem we consider, the required reference solutions for the homogeneous body can be found in a number of books such as Timoshenko and Goodier (1970), Sneddon (1951) and Neuber (1937). For example, the total applied force $F$ is related to the vertical displacement $t_0$ (Fig. 2) of the punch by

$$t_0 = \frac{F}{4a}\frac{1-\nu}{\mu}. \tag{1}$$

Now the question is how the force $F$ and the vertical displacement of the punch $t$ will be

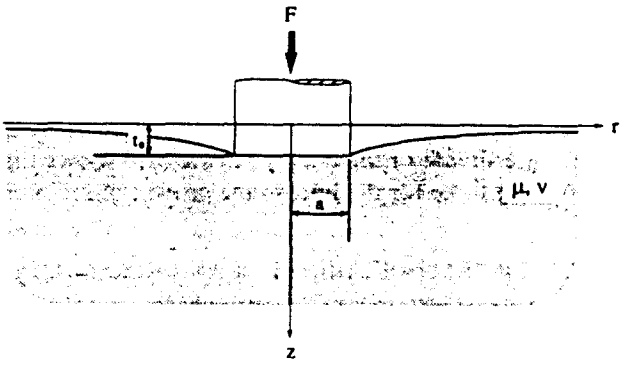


Fig. 2. A rigid cylindrical punch indenting a homogeneous half space.

related in the case of a layered material as in Fig. 1(b). The exact answer to this question would require numerical calculations, but we derive a closed-form, first-order-accurate solution to the problem.

*Moduli-perturbation analysis*

Consider the elastic contact problem in Fig. 1(b). The film/substrate medium can be viewed as a homogeneous body made entirely of the substrate material subjected to a phase transformation in the film region $0 < z < h$. During the transformation, the applied force $F$ is kept constant but the vertical displacement $t$ and the strain energy are allowed to change. Energy conservation law requires that the extra work done by the force $F$ be equal to the energy change in the whole body. To the first-order accuracy in the moduli variation, the equation of energy conservation reads

$$\tfrac{1}{2}F\delta t_0 = -\tfrac{1}{2}\int_{V_f} \delta c_{ijkl} u^0_{i,j} u^0_{k,l}\, dV, \tag{2}$$

where $\delta t_0$ is the displacement change, $\delta c_{ijkl} = c^f_{ijkl} - c^s_{ijkl}$ denotes the change in elastic moduli from originally pure substrate material to the present nonhomogeneous film/substrate medium, and $u^0_i$ is the known displacement solution for the reference homogeneous body in Fig. 2. The right-hand side of eqn (2) denotes the first order energy variation due to a moduli transformation [e.g. Eshelby (1970)]. For isotropic solids, $\delta c_{ijkl}$ can be rearranged as

$$\delta c_{ijkl} = e\lambda_s \delta_{ij}\delta_{kl} + \frac{\Delta\mu}{\mu_s} c^s_{ijkl}, \tag{3}$$

where $\lambda_s$ is the Lamé constant of the substrate, $\Delta\mu = \mu_f - \mu_s$ and

$$e = \frac{\Delta\lambda}{\lambda_s} - \frac{\Delta\mu}{\mu_s} = \frac{\mu_f}{\mu_s}\cdot\frac{(\nu_f - \nu_s)}{\nu_s(1-2\nu_f)}. \tag{4}$$

Substituting (3) into (2) and invoking the divergence theorem to the second term in the integral lead to the following expression for $\delta t_0/t_0$,

$$\frac{\delta t_0}{t_0} = -\frac{e\lambda_s}{Ft_0}\int_{V_f} \varepsilon^0_{jj}\varepsilon^0_{kk}\, dV - \frac{\Delta\mu}{Ft_0\mu_s}\int_{A_f} \sigma^0_{ij} n_i u^0_j\, dA, \tag{5}$$

where $V_f$ and $A_f$ denote the domain volume and the boundary surface of the transforming (film) region. Summation over repeated indices will always be implied in the paper. For the present film/substrate geometry, $A_f$ consists of two horizontal planes $z = 0$ and $z = h$, and the area integral on the plane $z = 0$ is equal to $Ft_0$. Thus, eqn (5) reduces to

$$\frac{\delta t_0}{t_0} = -\frac{e\lambda_s}{Ft_0}\int_{V_f} \varepsilon^0_{jj}\varepsilon^0_{kk}\, dV - \frac{\Delta\mu}{\mu_s}\left[1 + \frac{2\pi}{Ft_0}\int_0^\infty (\sigma^0_{zz}u^0_z + \sigma^0_{rz}u^0_r)_{z=h} r\, dr\right]. \tag{6}$$

Substituting the reference elastic contact solutions for punches on a homogeneous body [e.g. Neuber (1937)] into eqn (6), the two integrals are found to be

$$\frac{e\lambda_s}{Ft_0}\int_{V_f} \varepsilon^0_{jj}\varepsilon^0_{kk}\, dV = \frac{\mu_f(1-2\nu_s)(\nu_f-\nu_s)}{\mu_s(1-2\nu_f)(1-\nu_s)} I_1(\xi) \tag{7}$$

and

$$\frac{\Delta\mu}{\mu_s}\left[1+\frac{2\pi}{Ft_0}\int_0^\infty (\sigma_{zz}^0 u_z^0+\sigma_{rz}^0 u_r^0)_{z=h} r\,dr\right]=\frac{\mu_f-\mu_s}{\mu_s}I_0(\xi), \tag{8}$$

where $\xi = h/a$ and

$$I_1(\xi)=\frac{2}{\pi}\arctan\xi+\frac{\xi}{\pi}\ln\frac{1+\xi^2}{\xi^2} \tag{9}$$

$$I_0(\xi)=\frac{2}{\pi}\arctan\xi+\frac{1}{2\pi(1-\nu)}\left[(1-2\nu)\xi\ln\frac{1+\xi^2}{\xi^2}-\frac{\xi}{1+\xi^2}\right]. \tag{10}$$

The detailed calculations of the integrals are presented in the Appendix. Both $I_0$ and $I_1$ vanish as $\xi \to 0$ and approach unity as $\xi \to \infty$. The total vertical displacement $t$ can be written as $t = t_0+\delta t_0$, with the result

$$t(h/a)=\frac{F(1-\nu_s)}{4a\mu_s}\left[1-\frac{\nu_f-\nu_s}{1-\nu_s}I_1(h/a)-\frac{\mu_f-\mu_s}{\mu_s}I_0(h/a)\right] \tag{11}$$

to first order in the moduli variations, $\nu_f-\nu_s$ and $(\mu_f-\mu_s)/\mu_s$. The first order solution in eqn (11) reduces to the exact solution in the limit of $h/a \to 0$, corresponding to the case of a homogeneous half space made entirely of the substrate material.

The moduli perturbation can be achieved in two ways, from a homogeneous matrix by transformation in the film region $0 < z < h$, or alternatively, from a homogeneous film by transformation in the substrate region $h < z < \infty$. Thus, one could write another first order perturbation formula, similar to eqn (11) but based on the reference state of a homogeneous film. Within first order accuracy, the two perturbation formulae must agree with each other because they are both rigorous to first order in moduli difference. In the two limiting cases, i.e. as the geometric ratio $h/a$ approaches either zero or infinity, the displacement solution $t$ has the exact solution given in eqn (1) for a homogeneous half space. In order to retain the form of the exact solutions in both limiting cases, we combine the two first-order perturbation formulae into the following unified form

$$\begin{aligned} t(h/a)&=\frac{F(1-\nu_s)}{4a\mu_s}\left[1-\frac{\nu_f-\nu_s}{1-\nu_s}I_1(h/a)\right]\left[1+\frac{\mu_f-\mu_s}{\mu_s}I_0(h/a)\right]^{-1}\\ &=\frac{F}{4a}\cdot\frac{1-[\nu_f I_1+\nu_s(1-I_1)]}{\mu_f I_0+\mu_s(1-I_0)}. \end{aligned} \tag{12}$$

The modified perturbation solution for $t$ in eqn (12) perfectly matches the exact solutions in both limiting homogeneous cases, i.e. as $h/a \to 0$ and $h/a \to \infty$, and is equivalent to eqn (11) within first order accuracy. By comparing with results obtained from numerical computations, it has been found that eqn (12) has a larger range of validity for moduli differences than eqn (11). Later, we will show that this solution is valid for a moderate range of material combinations of practical importance.

Equation (12) indicates that for a film/substrate medium the punch displacement $t$ is linearly dependent on the total force $F$ through some effective contact compliance modulus. This relation is, in spirit, consistent with those proposed in previous studies (Bhattacharya and Nix, 1988; King, 1987; Doerner and Nix, 1986). However, it has been previously assumed that the effective contact compliance can be written as a linear combination of those of the film and substrate weighted by a fraction coefficient $\hat{I}(h/a)$, i.e. (Bhattacharya and Nix, 1988; King, 1987)

$$\left(\frac{1-\nu}{\mu}\right)_{\text{eff}} = \left(\frac{1-\nu}{\mu}\right)_{\text{f}} \hat{I}(h/a) + \left(\frac{1-\nu}{\mu}\right)_{\text{s}} [1-\hat{I}(h/a)]. \tag{13}$$

In contrast, eqn (12) shows that, to at least first-order accuracy, the effective contact compliance should have the form

$$\left(\frac{1-\nu}{\mu}\right)_{\text{eff}} = \frac{1-\nu_{\text{s}}-(\nu_{\text{f}}-\nu_{\text{s}})I_1(h/a)}{\mu_{\text{s}}+(\mu_{\text{f}}-\mu_{\text{s}})I_0(h/a)}, \tag{14}$$

which is equivalent to choosing the "effective" Poisson's ratio $\nu_{\text{eff}}$ and "effective" shear modulus $\mu_{\text{eff}}$ as

$$\nu_{\text{eff}} = \nu_{\text{s}}+(\nu_{\text{f}}-\nu_{\text{s}})I_1(h/a), \qquad \mu_{\text{eff}} = \mu_{\text{s}}+(\mu_{\text{f}}-\mu_{\text{s}})I_0(h/a). \tag{15, 16}$$

Further examination of the two weighting functions $I_0$ and $I_1$ reveals some interesting features of the effective constants $\nu_{\text{eff}}$ and $\mu_{\text{eff}}$ as defined in (15) and (16). It can be seen from eqn (8) that $I_0$ gives the ratio of the strain energy stored in the transforming (film) region to the total strain energy stored in the half space. Hence, it can be said that $\mu_{\text{eff}}$ is an average shear modulus weighted by the strain energy density distribution. On the other hand, $I_1$ can be rewritten as

$$I_1 = \frac{\lambda+2\mu}{E}\frac{1}{Ft_0}\int_{V_{\text{f}}} \sigma_{kk}\varepsilon_{jj}\,\mathrm{d}V,$$

which gives the ratio of the dilatational strain energy stored in the transforming (film) region to the total dilatational strain energy. In other words, $I_1$ is proportional to the hydrostatic part of the strain energy stored in the film region before moduli-transformation. Thus, it can be said that $\nu_{\text{eff}}$ in (16) is an average Poisson ratio weighted by the dilatational strain energy distribution.

Some ambiguities (higher than first order) arise in determining $\mu_{\text{eff}}$, in that the function $I_0$ depends on the Poisson ratio $\nu$ which can be taken as either the film or the substrate value. However, this is found to have a negligible effect because both $I_0$ and $\mu_{\text{eff}}$ are rather insensitive to the choice of $\nu$. As shown in Fig. 3, when $\nu$ is allowed to vary between 0.2 and 0.4 with $\mu_{\text{s}}/\mu_{\text{f}}$ between 1/2 and 2, the variation of $I_0$ is less than 8% and that of $\mu_{\text{eff}}$ is

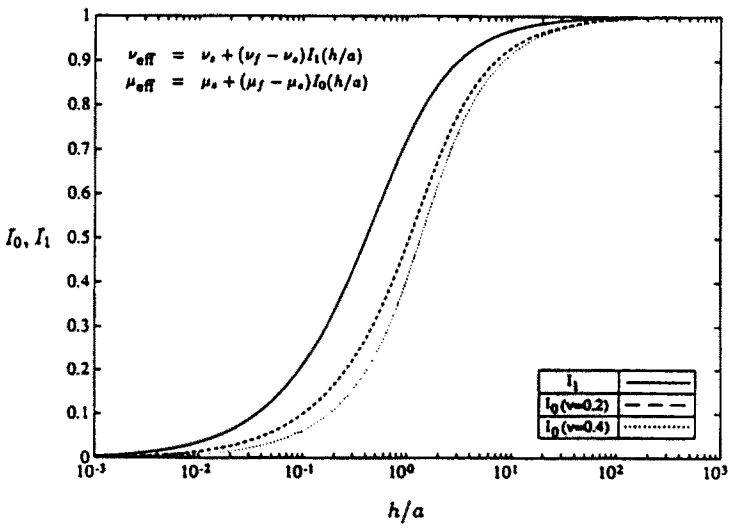


Fig. 3. The weighting functions $I_0$ and $I_1$ of eqns (9) and (10).

within 6.5%. Specifically, for the Aluminum thin film on Silicon substrate, the variations are within 1%. [The material constants of Al and Si are listed in Bhattacharya and Nix (1988), Table 2.] Hence, the ambiguity resulting from the $\nu$ dependence of $I_0$ can be neglected, at least in the range $0.5 < \mu_s/\mu_f < 2$ and $0.2 < \nu_{f,s} < 0.4$. Figure 3 also indicates that $I_1$ approaches unity faster than $I_0$, implying that the substrate has a greater influence on $\mu_{\text{eff}}$ than on $\nu_{\text{eff}}$. For instance, when the contact radius is one third of the film thickness (i.e. $h/a = 3$), the substrate has only 10% influence on $\nu_{\text{eff}}$ in comparison with about 25% influence on $\mu_{\text{eff}}$.

*Application to microindentation of thin films on substrate*

Equation (12) can be used to determine the unloading compliance of a conical or pyramidal indenter penetrating a thin film on substrate, as a function of the plastic indentation depth $t_p$ [Fig. 1(a)]. Requiring that the elastic contact area $\pi a^2$ be equal to the projected area of the penetration region of the actual indenter yields a relation between the elastic contact radius $a$ and the plastic depth $t_p$. For a conical indenter, that relation is simply $t_p = a/\tan\phi$ where $\phi$ is the half internal angle of the cone. Other indenter shapes such as a pyramidal indenter can be converted to an equivalent conical indenter by the same equal projection principle. Therefore, the unloading compliance of a conical indenter is

$$\frac{dt}{dF} = \frac{1}{4t_p \tan\phi}\left(\frac{1-\nu}{\mu}\right)_{\text{eff}}, \tag{17}$$

where the effective contact modulus is given by (14).

Figure 4 plots the unloading elastic compliance $h\,dt/dF$ vs $h/t_p$ as predicted by (17) for a conical indenter with $\phi = 68^\circ$ penetrating an Al thin film on Si substrate, in which the moduli of Al and Si are chosen as the same as those used by Bhattacharya and Nix (1988, Table 2). The corresponding results obtained from elastic-plastic FEM analysis by Bhattacharya and Nix (1988) and those predicted by King's (1987) integral equation analysis are also shown in the figure for comparison. Our first order solution appears to be in close agreement with the results from numerical computations. Compared with King's empirical formula, our solution is analytically rigorous to first-order accuracy in moduli differences. In this case, the shear moduli ratio is as large as 1.74, and the first-order moduli-perturbation analysis still provides a good estimate for the unloading compliance.

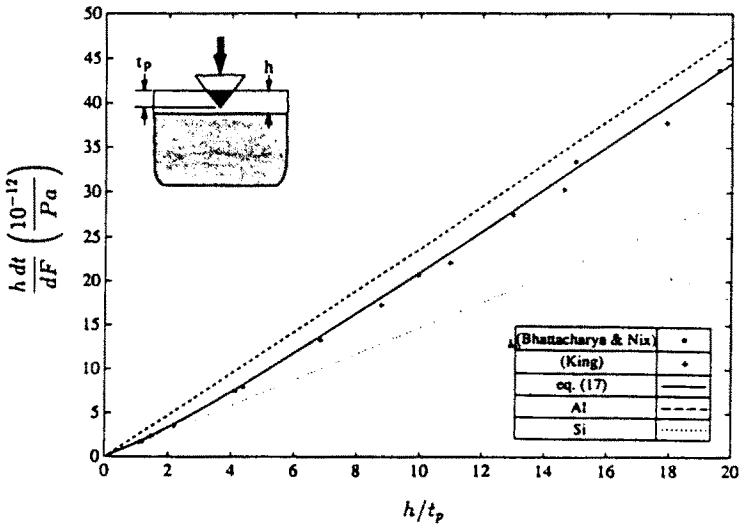


Fig. 4. Comparison of the unloading compliance $h\,dt/dF$ predicted by eqn (17), King (1987) and Bhattacharya and Nix (1988).

*Nonhomogeneous medium with piecewise constant or continuously varying moduli*

Our moduli-perturbation analysis provides a natural channel for extension to more complicated problems. Figure 7 depicts a substrate coated with $n$ elastically dissimilar films. Following similar steps as in (2)–(12), the first-order solution for the contact compliance can be obtained as

$$t = \frac{F}{4a} \cdot \frac{1-[1-I_1(h_n/a)]\nu_s - \sum_{i=1}^{n} [I_1(h_i/a) - I_1(h_{i-1}/a)]\nu_i}{[1-I_0(h_n/a)]\mu_s + \sum_{i=1}^{n} [I_0(h_i/a) - I_0(h_{i-1}/a)]\mu_i}, \tag{18}$$

where $h_i/a$ is defined in Fig. 7.

A rigorous analysis of error bounds for the perturbation formulae in eqns (12) and (18) is not yet available. It is thus necessary to examine the range of validity of the first order solutions through comparison with results obtained from numerical computations such as FEM analysis of a film/substrate medium with increasing moduli differences. (Detailed information about the meshes and elements used in our FEM calculations are presented in the next section.) Figure 5(a) plots the nondimensional compliance versus the shear modulus ratio $\mu_f/\mu_s$ for one layer of thin film on substrate with $\nu_f = \nu_s = 0.25$ and geometric aspect ratios $h/a = 0.5, 1, 3, 7$. We found that the results predicted by eqn (12) are within 7% of those predicted by FEM analysis for $0.5 < \mu_f/\mu_s < 2$ for all cases considered. The perturbation solution becomes increasingly accurate as $h/a$ increases. Figure 5(b) plots the same results for two different layers. For convenience, the shear modulus of the middle layer is taken to be the average of those of the top layer and the substrate. Compared with the one layer case in Fig. 5(a), a similar, slightly improved accuracy range for the perturbation solution is observed in this case. The effect of a different Poisson's ratio is also examined. Figure 6 plots $ht/F$ versus $\nu_f$ for $\mu_f/\mu_s = 2$, $\nu_s = 0.2$ and $h/a = 7$. In that case, the differences between the perturbation results and FEM results are about 5%. Thus, based on FEM calculations, the first order solution in eqn (12) appears to be within 7% error for $0.5 < \mu_f/\mu_s < 2$ and $0.2 < \nu_{f,s} < 0.4$. In fact, we find that the perturbation results agree fairly well (within around 15% error) with the FEM results for moduli ratio as large as 3. In that range, the linear elastic finite element calculations we adopt may themselves have significant errors. For example, as moduli difference increases, a hard film on relatively soft substrate behaves somewhat like an elastic beam on a soft elastic foundation, in which case the linear elastic finite elements are expected to underestimate the system compliance. More accurate finite element calculations with large deflection capabilities will be needed to fully resolve this problem.

The remarkable accuracy of the modified first order perturbation formula in eqns (12), (17) and (18) for moduli ratios up to 2 or 3 should not be considered as being just fortunate. It is known that properly rewriting a perturbation formula of the same order could result in a substantial increase in its range of validity. Numerous examples of success could be given. As an example known to the fluid mechanics research community, Shanks (1955) [see also Van Dyke (1975) for more discussions on the convergence properties of a perturbation series expansion] showed that by properly rewriting a perturbation solution for the drag of a sphere in the Oseen approximation for low Reynolds number ($R$) flow, the original perturbation solution, which is only valid for $R < 1$, can be converted to one which agrees well with more exact calculations up to $R = 10$. In a perturbation analysis of 3D planar cracks, Gao and Rice (1987) found their first order solution, when applied to an elliptical crack, is accurate within 5% up to an aspect ratio as large as 2. Our modified first order solution in eqn. (12) was obtained so that the form of the exact solutions is retained in both the limiting homogeneous cases, as $a/h \to 0$ and $a/h \to \infty$. It is known that properly matched perturbation solutions can often achieve remarkable agreement with exact calculations.

The general solution to a rigid punch indenting a nonhomogeneous material with continuously varying moduli $\mu(z)$ and $\nu(z)$ can also be constructed. Taking the limits as $h_i \to h_{i-1}$ and $n \to \infty$ in eqn (18), the final solution has the integral form

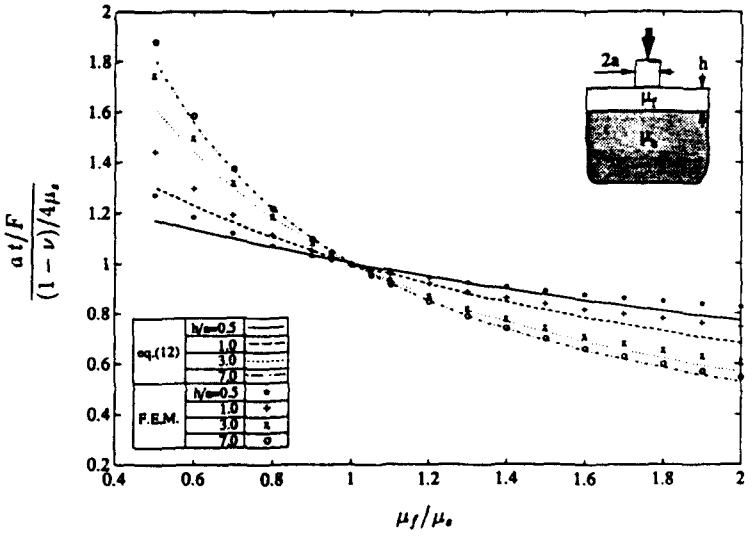


(a)

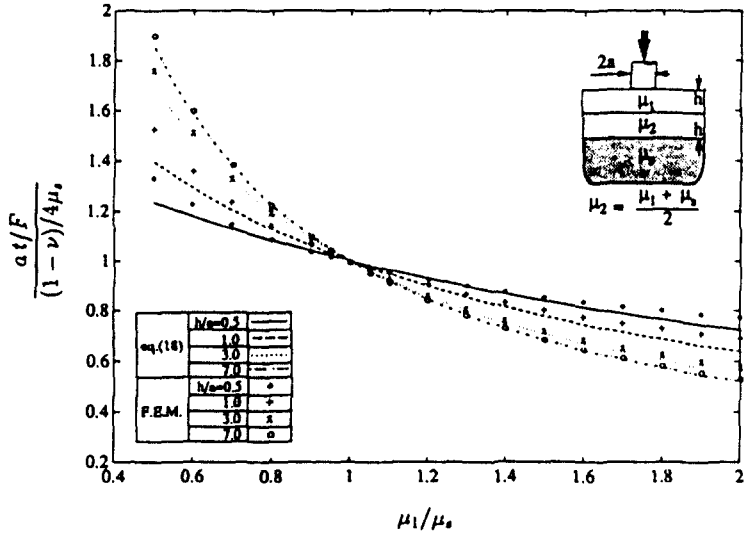


(b)

Fig. 5. Comparison of the perturbation solutions given in eqns (12) and (18) with finite element results: (a) one layer and (b) two layers.

$$t = \frac{F}{4a}\left[1 - \int_0^{\infty} \frac{\mathrm{d}I_1(z/a)}{\mathrm{d}z} v(z)\,\mathrm{d}z\right] \Big/ \int_0^{\infty} \frac{\mathrm{d}I_0(z/a)}{\mathrm{d}z} \mu(z)\,\mathrm{d}z. \tag{19}$$

Without further comparison with numerical results, we expect that these formulae have similar ranges of validity as eqn (12). Analogously, these solutions can be used to model the unloading process of indentation testing of a substrate with multi-layer coating or a nonhomogeneous solid with continuously varying elastic constants.

## EFFECTS OF A PENNY-SHAPED INTERFACIAL CRACK

*Finite element set-up*

In the previous section, closed-form first-order solutions have been derived for the elastic contact modulus of a layered medium. These solutions can be used to understand

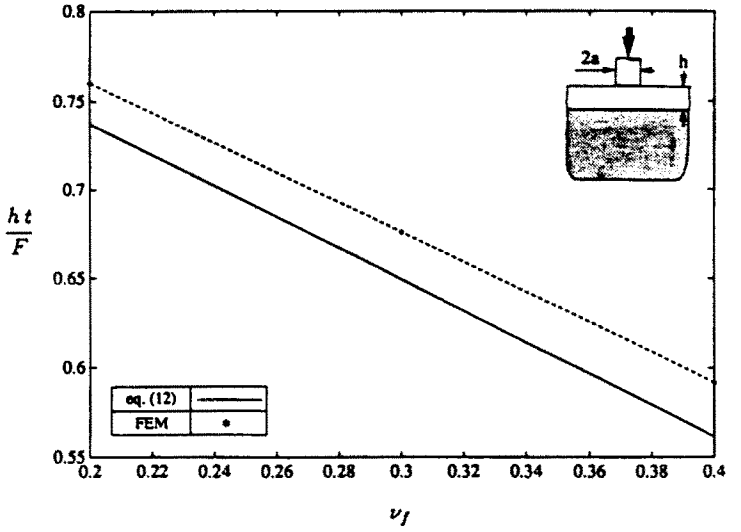


Fig. 6. Comparison of the perturbation solution with finite element results for different film Poisson ratio $\nu_f$ when $\nu_s = 0.2$ and $\mu_f/\mu_s = 2$.

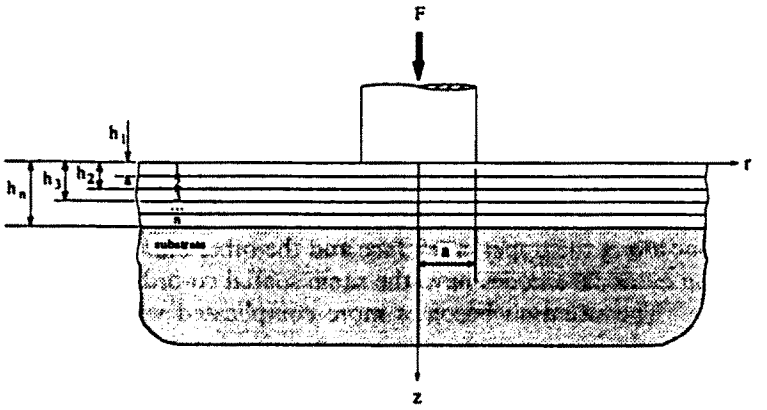


Fig. 7. A rigid cylindrical punch indenting a $n$-layer coating on substrate.

the effects of material inhomogeneity on the indentation of thin films deposited on substrate. However, as Wu *et al.* (1990a) pointed out, interfacial cracks may also come into play if the adhesion strength of the film/substrate interface is weak. The effect of such interfacial cracks on the contact compliance of the film/substrate and the crack-tip energy release rate are studied in this section. Wu *et al.* (1990a) observed that the measured unloading compliance of a film/substrate specimen may show a large discrepancy depending on the adhesion strength between the film and the substrate. In their experiment, two specimens of Al/Si are tested using a pyramidal indenter, one with a very strong interface bonding and the other with a weak bonding. It was suggested that an interfacial crack developed in the specimen with weaker interface, resulting in a dramatic increase in the unloading compliance. In response to this experiment, we carry out a FEM analysis to investigate the effect and behavior of such debonding cracks, based on the DLEARN finite element code (Hughes, 1987). For simplicity, we consider the geometry of an axisymmetric penny-shaped crack with radius $L$ along the film/substrate interface, as illustrated in Fig. 8. The crack surfaces will be allowed to slide without friction (although consideration of friction poses no essential difficulties to our numerical calculations).

As is known, several complications may arise in the finite element simulation of indentation contact. First, for our problem an infinitely large domain needs to be considered for complete elimination of boundary effects. In FEM analysis that is usually approximated

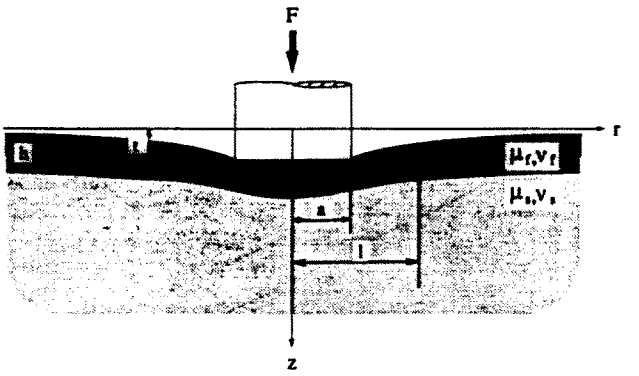


Fig. 8. A rigid cylindrical punch indenting a film/substrate medium containing a penny-shaped interface crack.

by taking a very large domain with displacements fixed around the boundary. This large domain size is essentially arbitrary as long as proper convergence can be achieved. The overall domain size is generally one or two orders of magnitude larger than any length scales involved in the problem. In anticipation, such an approach would require a large number of elements for elastic contact problems because the remote stress field decays only in the order $1/r$. Thus, we choose to adopt the so-called infinite element (Zienkiewicz *et al.*, 1983; Zienkiewicz, 1989) which simulates an infinite domain through a proper mapping function. A layer of infinity element is added outside our regular mesh domain which is taken to be about 10 times larger than the largest length scale among the punch radius ($a$), film thickness ($h$) and crack length ($L$).

The second problem emerges in simulating the crack face contact due to compressive loading. A common approach for traction-free, open crack surfaces is to distribute two arrays of nodes, one along the upper crack face and the other along the lower crack face. Two corresponding crack face nodes have the same spatial co-ordinates but independent degrees of freedom. The situation becomes more complicated when parts of the crack surfaces may be brought into contact under compressive loading, as in the indentation problem. In that case, crack face interpenetration may result if fully independent degrees of freedom are granted. To avoid this problem, the crack face nodes in contact should be constrained to move together in the normal direction, yet allowed to move freely relative to each other in the horizontal direction. In other words, the crack face nodes should be constrained differently depending on the local crack face configuration (open or closed). We adopt the so-called penalty method in which a spring element with very large stiffness is added between two separate crack face nodes to make them move together in the normal ($z$) direction. Our FEM procedure begins by setting up an array of normal spring elements for all crack face nodes. After the initial run, the normal traction along the crack face is computed and any nodes showing tensile traction are set free by removing the spring element at those nodes. This procedure is iterated until no tension is found along the crack surfaces. By doing so, it is guaranteed that the crack surfaces will open under tension but close to contact under compression.

Plastic deformation generated as the hard indenter penetrates into the film/substrate medium poses another complication to our analysis. A fully elastic–plastic FEM analysis is known to be very costly, especially if a large amount of information on different crack lengths and film thicknesses is desired. Since previous elastic calculations matched so well with the fully elastic–plastic FEM analysis by Bhattacharya and Nix (1988), one may anticipate that the plastic strain will not have significant effects on the largely elastic unloading process of an indentation test. Further support of this conclusion is provided by our FEM analysis which shows that a uniform dilatational residual strain, whose magnitude is determined by the volume of the penetrated indenter region, in the near neighborhood of a punch does not cause appreciable change in the elastic contact compliance. However, the residual strain in the debonded film due to plastic deformation may be a major source

for the energy release rate, as shown in the previous work by Evans and Hutchinson (1984). Sufficiently large residual stress may lead to buckling of the film. The reader is also referred to Hutchinson *et al.* (1992) for more recent work on the buckling-driven film delamination problems. Using a simple plane stress film delamination model, we provide estimates for the calculation of energy release rate at the interfacial crack tip, which is compared to a uniform stress model by Evans and Hutchinson (1984).

Figure 9 shows a typical axisymmetric FEM mesh used in our computation. In this figure, both the film thickness ($h$) and the punch radius ($a$) are assumed to be unity. The domain size with regular elements is taken to be $100 \times 20$ ($r \times z$) and a layer of infinity elements is distributed around the regular domain. The total node number reaches 2044.

A 9-node isoparametric element [Fig. 10(a)] is used for the overall domain and special singular elements (Barsoum, 1977) are adopted to account for the stress singularity at the punch and crack tip. The singular element is a triangular element [Fig. 10(b)] degenerated from the 9-node square element with transition of the mid-side nodes to quarter points. This element is known to have the same order of stress singularity throughout the element (Atluri, 1986). The symmetric boundary condition $u_r = 0$ is imposed at $r = 0$, and zero displacements ($u_r = u_z = 0$) are imposed at the infinity nodes via the mapping function in the infinity element.

With the above mesh and element set-up, a constant normal displacement ($t$) is imposed at $z = 0$ and $|r| \leqslant a$. The nodal stress values are obtained by the local least square method (Hinton and Campbell, 1974). These nodal stress values are then used to produce the total normal force under the punch by both cubic spline interpolation and 15 points Gauss Chebyshev integration rule. Finally the integrated total force is divided by the imposed displacement $t$ to yield the contact stiffness or compliance of the film/substrate composite. This FEM set-up can be tested by first considering an uncracked homogeneous body (Fig. 2). Comparing with the exact solution in eqn (20), the relative error of the FEM result for the contact compliance was found to be within 1% error.

We use Al thin film on the Si substrate in the FEM calculation. Table 1 lists the selected material constants of Al and Si. Four different ratios of contact radius to film thickness, $a/h = 0.2, 0.5, 1.0, 2.5$, will be considered. A proper analysis range of the crack size is chosen based on the stress distribution along the uncracked interface shown in Fig. 11. Note that the normal stress $\sigma_{zz}$ is always negative (compressive) while both normal and shear traction diminishes to nearly zero beyond a characteristic distance several times the film thickness, suggesting that the effects of interface debonding will quickly saturate as the

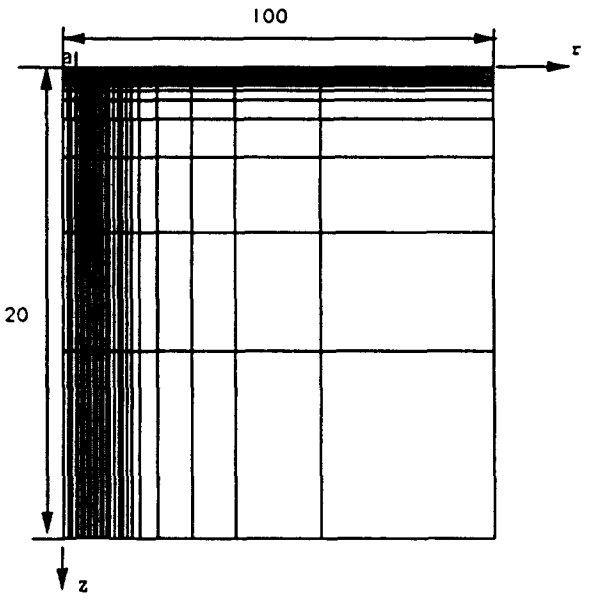


Fig. 9. The axisymmetric FEM mesh.

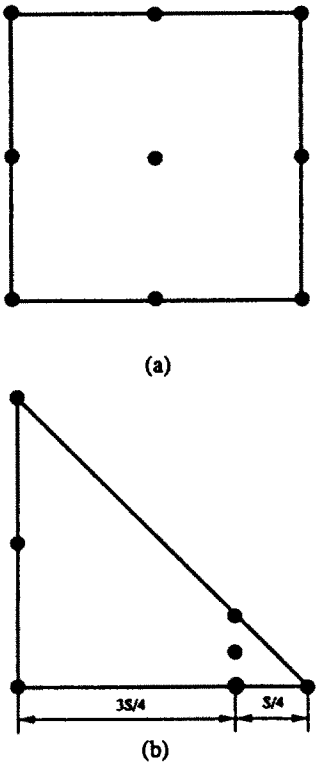


Fig. 10. (a) A 9-node isoparametric element and (b) a quarter-node singular element.

crack extends beyond that characteristic distance. Guided by this observation, we performed the FEM computation for $L/h$ values lying in the range with significant interface traction distribution.

A uniform dilatation with magnitude equal to the penetrated indenter volume was imposed in the region $0 < z < h$ (Fig. 15) and $0 < r < a$ to represent the plastic deformation generated during penetration. All calculations were carried out for both with and without the presence of the dilatational strain. A total of 36 cases were run on a Convex computer. The CPU time was about 3 min for each run.

*Effect of interface cracking on contact compliance*

The calculated contact compliance ($C$) will be normalized with respect to that of the film (Al) material ($C_f$),

$$C_f = (1-\nu_f^2)/(2E_f a). \tag{20}$$

The normalized compliance $C/C_f$ is plotted in Fig. 12 as a function of the crack length $L/h$. The calculated values are shown as dot points. The solid lines are obtained by cubic spline interpolation of the FEM results. In all cases considered, with or without interfacial crack, the dilatational strain does not appear to cause any appreciable changes in the contact compliance value. Thus, in consistency with the previous elastic–plastic FEM analysis by Bhattacharya and Nix (1988), our calculations provide further evidence that the plastic effects can be neglected in estimating the unloading indentation compliance of a thin film on substrate.

Table 1. Material properties of Al and Si

| | $E$ (Gpa) | $\nu$ |
|---|---|---|
| Al | 71.391 | 0.347 |
| Si | 165.89 | 0.218 |

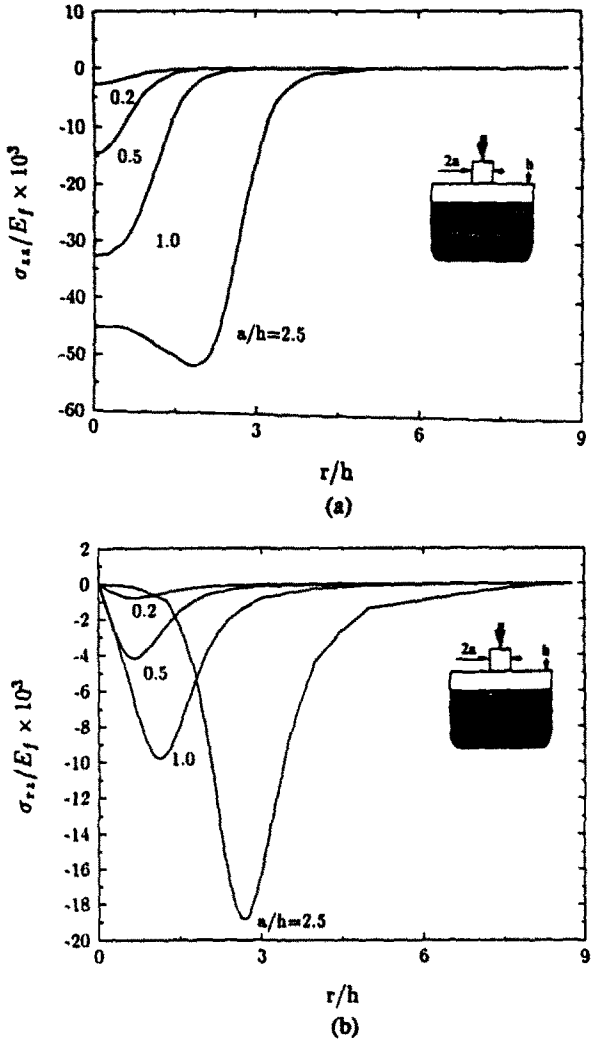


Fig. 11. Distribution of (a) normal stress $\sigma_{zz}$ and (b) shear stress $\sigma_{rz}$ along the film/substrate interface.

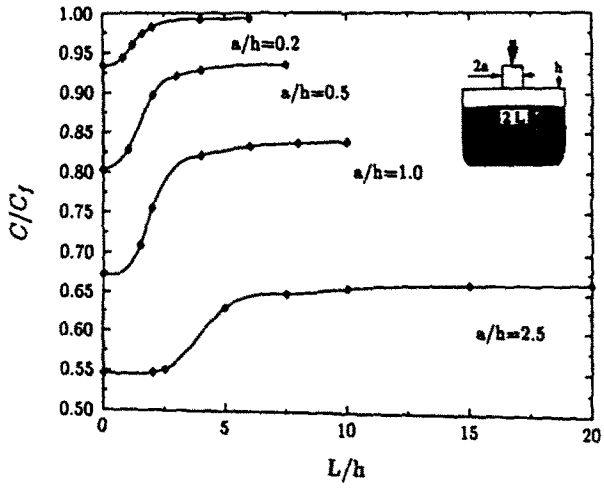


Fig. 12. Variation of contact compliance with crack length.

The previous perturbation solution showed that the effect of substrate increases with the contact aspect ratio $a/h$. Our FEM results reaffirm this tendency. Without cracking, the contact compliance of the Al/Si system is around 93% that of Al for $a/h = 0.2$, and it drops to only 67% for $a/h = 1.0$. This appears to be in reasonable agreement with the experimental result of Wu *et al.* (1990a).

Figure 12 shows that the contact compliance quickly approaches a constant value as the crack size reaches a characteristic length which, for convenience, will be referred to as the elastic saturation crack size. The saturation crack size ranges from a few times the film thickness for small $a/h$ values such as 0.2 to about 20 times for relatively large $a/h$ values such as 2.5. The presence of an interface crack increases the contact compliance by up to 7.2% when $a/h = 0.2$ and up to 25% when $a/h = 1.0$, corresponding to stiffness reductions of 6% and 20%, respectively. These results can be compared with the experimental observations of Wu *et al.* (1990a). These authors measured the contact stiffness values using a pyramidal indenter of internal angle 77° which, according to the principle of equal contact area projection, is equivalent to a conical indenter with half internal angle $\phi = 70°$. Figure 13 plots our FEM values for the contact stiffness at different $t_p/h$ for the Al/Si system in the limits of zero and saturation crack length. Compared with our results, Wu *et al.* (1990a) observed a slightly larger stiffness reduction due to cracking (about 32% in the case $a/h = 1.0$). Other than possible experimental fluctuations and the approximations adopted in our contact model, this difference may be attributed possibly to additional cracking normal to the interface due to indenter penetration.

*Estimates for the crack-tip energy release rate*

The driving force for the interfacial crack comes mainly from two sources. First, the force $F$ on the indenter causes elastic strain energy stored in the body, which may be partly released as debonding occurs. Second, the energy stored as residual strain in the body due to the plastic deformation generated during penetration of the indenter may be released as the debonding crack grows along the interface. For ease of discussion, we shall refer to them as the elastic and plastic strain contributions, respectively.

The elastic contribution $G^e$ to the energy release rate can be calculated from the change in the contact compliance $C$ (Kanninen and Popelar, 1985, p. 160) of the body with respect to the crack size enlargement. We adopt a more accurate calculation using the virtual crack extension method (Parks, 1974), with results plotted in Fig. 14. It is observed that $G^e$ first reaches a maximum peak and then diminishes to zero as the crack size exceeds a saturation length, in consistency with the behavior of the contact compliance.

The plastic strain contribution $G^p$ to the energy release rate can be estimated using a plane stress model in which the debonded thin film is treated as a thin circular plate, as in Evans and Hutchinson (1984). We hasten to point out that our calculations indicate that

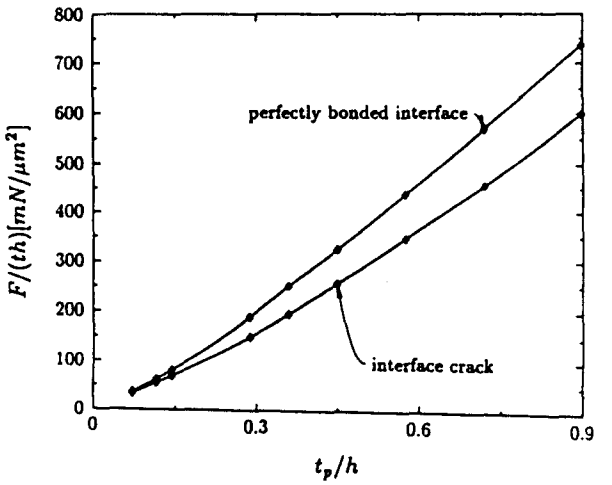


Fig. 13. Variation of contact stiffness $F/th$ with plastic depth $t_p/h$.

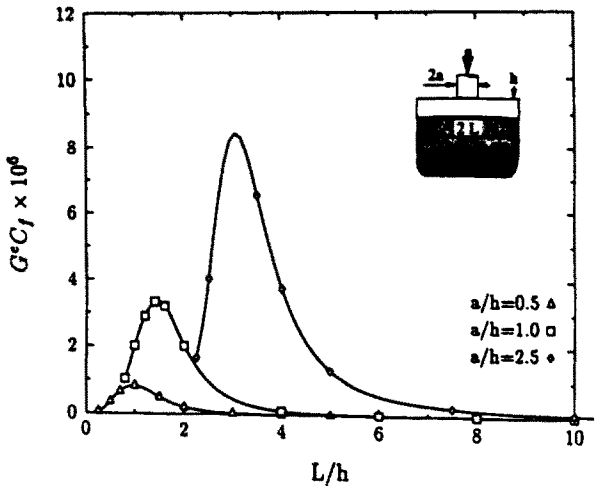


Fig. 14. Energy release rate at the crack tip in the absence of plastic deformation.

$G^p$ is at least two orders of magnitude larger than $G^e$, suggesting that the elastic deformation can be essentially ignored as far as the energy release rate calculation is concerned.

Evans and Hutchinson (1984) approximated the debonding film as a thin circular elastic plate clamped on the edge and subjected to a uniform biaxial strain caused by the indenter volume squeezed into the film. Their result, when specialized to our geometry, yields

$$G^p = \frac{\mu_f(1+\nu_f)a^6}{18(1-\nu_f)\tan^2\phi\, hL^4}. \tag{21}$$

Such a uniform stress model ignored the stress variation in the film. A more realistic model would incorporate the actual plastic zone. Here we adopt a slightly different model to estimate the plastic strain contribution $G^p$. Figure 15 shows the geometry of our model for a film debonded along a circular region of radius $L$. The debonded film can be divided into two characteristic regions. For simplicity, the inner region $r < a$ is taken to be the plastic zone in which the film is subjected to a volume expansion equal to the penetrated indenter volume, and is constrained by the punch at $z = h$ and by the substrate at $z = 0$. In the annular region $a < r < L$, the film is treated as a thin elastic plate clamped at $r = L$.

The following boundary conditions are imposed on the annular region $a < r < L$:

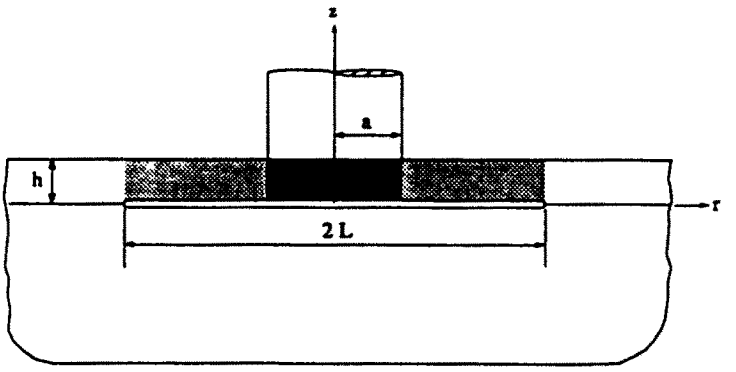


Fig. 15. Schematic diagram of a film debonded from a substrate along a circular area of radius $L$ and subjected to a dilatational strain $\varepsilon_0$ in the region $r < a$.

$$u_r = 0 \quad \text{at } r = L, \qquad u_r = u_1 \quad \text{at } r = a, \tag{22, 23}$$

where $u_1$ represents the radial displacement due to the dilatation within the inner plastic region, $0 < r < a$, where the boundary conditions are taken to be

$$u_z = -\varepsilon_0 h \quad \text{at } z = h, \qquad u_z = 0 \quad \text{at } z = 0, \qquad u_r = u_1 - \varepsilon_0 a \quad \text{at } r = a, \tag{24–26}$$

where $\varepsilon_0$ represents the dilatational strain caused by plastic deformation. Here $u_r$ and $u_z$ refer to the elastic part of the displacement field. The continuity of the total displacement in the radial direction has been imposed at $r = a$ through the condition (26). The above boundary value problem can be solved following the standard method. Requiring $\sigma_{rr}$ to be continuous at $r = a$ gives

$$u_1 = \frac{(1-\nu_f^2)(L^2-a^2)a\varepsilon_0}{2[L-\nu_f(L-a)][L-\nu_f(L+a)]}. \tag{27}$$

The strain energy $W$ stored in the whole debonded region of the film is calculated to be

$$W = \frac{\pi\mu_f(1+\nu_f)\varepsilon_0^2 h a^2[2L^2+a^2-2\nu_f(L^2-a^2)]}{[L-\nu_f(L-a)][L-\nu_f(L+a)]}. \tag{28}$$

Differentiating $W$ with respect to the crack radius $L$ and dividing the result by $2\pi L$ yields the energy release rate $G^p$,

$$G^p = \frac{\mu_f(1-\nu_f)(1+\nu_f)^2\varepsilon_0^2 h a^4}{[L-\nu_f(L-a)]^2[L-\nu_f(L+a)]^2}. \tag{29}$$

For a conical indenter with angle $2\phi$, the dilatational strain $\varepsilon_0$ is approximated as $a/(9h\tan\phi)$. Assuming $L \gg a$, we find

$$G^p = \frac{\mu_f(1+\nu_f)^2 a^6}{81(1-\nu_f)^3\tan^2\phi\, hL^4}. \tag{30}$$

Interestingly, this expression differs from the solution of Evans and Hutchinson, eqn (21), only by a factor $2(1+\nu_f)/[9(1-\nu_f)^2]$ which is about 0.70 when $\nu_f = 0.347$ for Al.

The boundary condition (24) assumes that the film is fully constrained in the vertical direction. This may be unrealistic because some relaxation in the vertical direction may be possible as the indenter penetrates into the film. Alternatively, we consider a traction-free condition at $z = h$. In that case, the same calculation procedure leads to

$$G^p = \frac{\mu_f(1+\nu_f)^2 a^6}{81(1-\nu_f)\tan^2\phi\, hL^4}, \tag{31}$$

which differs from eqn (30) by a factor $1/(1-\nu_f)^2$.

Curiously, eqns (21), (30) and (31) all suggest that $G^p \sim a^6 L^{-4} h^{-1}$ (or $t_p^6 L^{-4} h^{-1}$). These solutions are essentially of the same order with slightly different coefficients. Our FEM calculation also gives similar results which are found to lie in the range between those predicted by eqns (30) and (31). Substituting typical geometrical and material constants into eqns (21), (30) and (31) indicates that the value of $G^p$ is at least two orders of magnitude larger than the elastic contribution $G^e$ calculated by FEM, as presented in Fig. 14. Thus, we conclude that the plastic deformation does not cause appreciable changes in the elastic contact compliance, but it plays a major role in the energy release rate which drives the growth of a debonding crack.

## SUMMARY

In this paper we have addressed certain aspects of an elastic punch contact problem arising in modeling indentation tests of a layered material. First, a first order moduli-perturbation method has been used to derive closed-form elastic solutions, as given in eqns (12), (18) and (19), for the contact compliance of a nonhomogeneous solid with piecewise constant or continuously varying moduli. The perturbation solutions are rigorously valid to the first-order accuracy in the moduli variation. Comparing with numerical results in the literature, our solution has the advantage of being (i) in closed-form, (ii) first-order rigorous and (iii) easy to extend to more complicated elastic contact problems for a nonhomogeneous material. The perturbation solutions are used to estimate the unloading compliance associated with an indentation test of Al thin film on Si substrate. The result appears to be in good agreement with the elastic–plastic finite element analysis of Bhattacharya and Nix (1988). The range of validity of perturbation solutions has been further examined through comparison with numerical results obtained from a finite element analysis. It is found that the perturbation solutions are approximately valid (within 7% of FEM results) at least for moduli ratio up to 2.

Further, we perform a linear finite element analysis to examine the effects of an interface debonding crack on the contact compliance and to compute the energy release rate at the crack tip. Important conclusions are:

(1) Interface cracks can cause a significant increase in the contact compliance of a layered medium.
(2) There exists a saturation crack size beyond which the contact compliance no longer changes significantly with the crack length.
(3) The plastic strain near the indenter does not cause appreciable changes in the unloading compliance, but it plays a dominant role in interface debonding by providing a long range energy release rate which drives the crack growth.

*Acknowledgements*—It is with great pleasure that financial support is acknowledged, from IBM Almaden Research Center by a research initiation grant to H. Gao and a graduate fellowship to C. Chiu. The work of J. Lee was supported by NSF-MRL program through the Center for Material Research at Stanford University. We are extremely grateful to many helpful discussions throughout the course of the work with Dr T. W. Wu at IBM Almaden Research Center.

## REFERENCES

Atluri, S. N. (1986). *Computational Methods in the Mechanics of Fracture*. Vol. 2, pp. 170–227. North-Holland, Amsterdam.

Barsoum, R. S. (1977). Triangular quarter-point elements as elastic and perfectly-plastic crack tip elements. *Int. J. Num. Meth. Engng* **11**, 85–98.

Bhattacharya, A. K. and Nix, W. D. (1988). Analysis of elastic and plastic deformation associated with indentation testing of thin films on substrates. *Int. J. Solids Structures* **24**(12), 1287–1298.

Doerner, M. F. and Nix, W. D. (1986). A method for interpretating the data from depth-sensing indentation instruments. *J. Mater. Res.* **1**(4), 601–609.

Eshelby, J. D. (1970). Energy relations and the energy-momentum tensor in continuum mechanics. In *Inelastic Behavior of Solids* (Edited by M. F. Kanninen *et al.*), pp. 77–115. McGraw-Hill, Scarborough, CA.

Evans, A. G. and Hutchinson, J. W. (1984). On the mechanics of delamination and spalling in compressed films. *Int. J. Solids Structures* **20**(5), 455–466.

Gao, H. (1989). Weight functions for external circular cracks. *Int. J. Solids Structures* **25**, 107–127.

Gao, H. (1991). Fracture analysis of nonhomogeneous material via a moduli-perturbation approach. *Int. J. Solids Structures* **27**, 1663–1682.

Gao, H. and Rice, J. R. (1987). Somewhat circular tensile cracks. *Int. J. Fract.* **33**, 155–174.

Henshell, R. D. and Shaw, K. G. (1975). Crack tip finite elements are unnecessary. *Int. J. Num. Meth. Engng* **9**, 495–507.

Hinton, E. and Campbell, J. S. (1974). Local and global smoothing of discontinuous finite element functions using a least squares method. *Int. J. Num. Meth. Engng* **8**, 461–480.

Hughes, T. J. R. (1987). *The Finite Element Method*. Prentice-Hall, Englewood Cliffs, NJ.

Hutchinson, J. W., Thouless, M. D. and Liniger, E. G. (1992). Growth and configurational stability of circular buckling-driven film delaminations. *Acta Metall. Mater.* **40**, 295–308.

Kanninen, M. F. and Popelar, C. H. (1985). *Advanced Fracture Mechanics*. Oxford University Press, New York; Clarendon Press, Oxford.

King, R. B. (1987). Elastic analysis of some punch problems for a layered medium. *Int. J. Solids Structures* **23**, 1657–1664.

Laursen, T. A. and Simo, J. C. (1992). A study of the mechanics of microindentation using finite elements. *J. Mater Res.* **7**, 618–626.
Loubet, J. L., Georges, J. M., Marchesini, O. and Meille, G. (1984). Vickers indentation curves of magnesium oxide (MgO). *J. Tribology* **106**, 43–48.
Neuber, H. (1937), *Kerbspannungslehre*. Springer, Berlin (1946, English translation, Edwards Bros, Ann Arbor, Michigan).
Parks, D. M. (1974). A stiffness derivative finite element technique for determination of crack tip stress intensity factors. *Int. J. Fract.* **10**, 487–502.
Shanks, D. (1955). Non-linear transformations of divergent and slowly convergent sequences. *J. Math. Phys.* **34**, 1–42.
Shield, T. W. and Bogy, D. B. (1989). Some axisymmetric problems for layered elastic media: part I—multiple region contact solutions for simply-connected indenters. *J. Appl. Mech.* **56**, 798–806.
Sneddon, I. N. (1951). *Fourier Transform* (1st edn). McGraw-Hill, New York.
Timoshenko, S. P. and Goodier, J. N. (1970). *Theory of Elasticity* (3rd edn). McGraw-Hill, New York.
Van Dyke, M. (1975). *Perturbation Methods in Fluid Mechanics* (2nd edn). The Parabolic Press, Stanford, California.
Wu, T. T. (1991). Microscratch and load relaxation tests for ultrathin films. *J. Mater. Res.* **6**, 407–426.
Wu, T. W., Moshref, M. and Alexopoulos, P. S. (1990a). The effect of the interfacial strength on the mechanical properties of aluminum films. *Thin Solid Films* **187**, 295–307.
Wu, T. W., Shull, A. L. and Lin, J. (1990b). Microscratch test on carbon films as thin as 20 nm. *Mater. Res. Soc. Symp. Proc.* **188**, 207–212.
Yu, H. Y., Sanday, S. C. and Rath, B. B. (1990). The effect of substrate on the elastic properties of films determined by the indentation test—axisymmetric Bousinesq problem. *J. Mech. Phys. Solids* **38**, 745–764.
Zienkiewicz, O. C. (1989). *The Finite Element Method* (4th edn). McGraw-Hill, London.
Zienkiewicz, O. C., Emson, C. and Bettess, P. (1983). A novel boundary infinity element. *Int. J. Num. Meth. Engng* **19**, 393–404.

## APPENDIX: CALCULATION OF INTEGRALS FOR $I_0$ AND $I_1$

In the following, we will evaluate the key functions $I_0$ and $I_1$ in eqns (7) and (8) of the text:

$$I_0(h/a) = 1 + \frac{2\pi}{Ft_0}\int_0^\infty (\sigma_{zz}u_z + \sigma_{rz}u_r)_{z=h} r\,dr, \qquad I_1(h/a) = \frac{\mu_s(1-2\nu_f)(1-\nu_s)}{\mu_f(1-2\nu_s)(\nu_f-\nu_s)}\frac{e\lambda_s}{Ft_0}\int_{V_f} \varepsilon_{kk}^2\,dV. \tag{A1, A2}$$

Here for conciseness we have ignored the superscript 0 for quantities pertaining to the homogeneous half space, as it appeared in eqns (7) and (8). The homogeneous solutions for $u_z$, $u_r$, $\sigma_{zz}$ and $\sigma_{rz}$ to the punch contact problem can be determined from the Neuber's potential $\hat{G}$ (Neuber, 1937; Gao, 1989):

$$u_r = \frac{t_0}{\pi(1-\nu)a}[(1-2\nu)\hat{G}_{,r} + z\hat{G}_{,rz}], \qquad u_z = -\frac{t_0}{\pi(1-\nu)a}[2(1-\nu)\hat{G}_{,z} - z\hat{G}_{,zz}] + t_0, \tag{A3, A4}$$

$$\sigma_{rz} = \frac{2\mu t_0}{\pi(1-\nu)a} z\hat{G}_{,rzz}, \qquad \sigma_{zz} = -\frac{2\mu t_0}{\pi(1-\nu)a}[\hat{G}_{,zz} - z\hat{G}_{,zzz}], \tag{A5, A6}$$

where the constants $a$ and $t_0$ are the radius and the vertical displacement of the indenter. To carry out the integrals in (A1) and (A2), it is convenient to express the Neuber's potential $\hat{G}$ in the oblate spheroidal coordinates $(s, t)$ (Neuber, 1937; Gao, 1989)

$$\hat{G} = a^2\left\{\frac{z}{a}\arctan(\sinh s) + \sin t - \ln[\cosh s(1+\sin t)]\right\}, \tag{A7}$$

where $(s, t)$ are related to the cylindrical coordinate $(r, z)$ by

$$r + iz = a\cosh(s + it). \tag{A8}$$

*Function $I_0$*

Applying variable transformation $\xi = \sinh s$ to (A1) and denoting $\xi_0 = h/a$, $I_0$ can be rewritten as

$$I_0(\xi_0) = 1 + \frac{2\pi a^2}{Ft_0}\int_{\xi_0}^\infty (\sigma_{zz}u_z + \sigma_{rz}u_r)_{z=h}\left(\frac{\xi_0^2+\xi^4}{\xi^3}\right)d\xi. \tag{A9}$$

Substituting eqns (A3)–(A7) into (A9) leads to

$$I_0(\xi_0) = \frac{1}{\pi(1-\nu)}\int_{\xi_0}^\infty (g_1 - g_2 + g_3)\,d\xi, \tag{A10}$$

where

$$g_1 = \frac{2(1-\nu)}{a}\hat{G}_{,z}(\hat{G}_{,zz} - z\hat{G}_{,zzz})\left(\frac{\xi_0^2+\xi^4}{\xi^3}\right),$$

$$= \frac{2(1-\nu)(3\xi^6\xi_0^3 + 5\xi^4\xi_0^3 - \xi^2\xi_0^5 + \xi_0^5)\arctan\xi}{\xi^2(\xi^4+\xi_0^2)^2}, \tag{A11}$$

$$g_2 = \frac{z\hat{G}_{,zz}}{a}(\hat{G}_{,zz} - z\hat{G}_{,zzz})\left(\frac{\xi_0^2+\xi^4}{\xi^3}\right),$$

$$= \frac{\xi_0^2(3\xi^6\xi_0^3 + 5\xi^4\xi_0^3 - \xi^2\xi_0^5 + \xi_0^5)}{\xi(\xi^4+\xi_0^2)^3}, \tag{A12}$$

$$g_3 = z\hat{G}_{,zzz}\left[\frac{(1-2\nu)\hat{G}_{,z}}{a} + \frac{z\hat{G}_{,zz}}{a}\right]\left(\frac{\xi_0^2+\xi^4}{\xi^3}\right),$$

$$= \frac{-\xi_0^2(3\xi^4-\xi_0^2)[-(1-2\nu)\xi^5 + 2(1-\nu)\xi^4\xi_0 - (1-2\nu)\xi\xi_0^2 + (1-2\nu)\xi_0^3 - \xi^2\xi_0^3]}{\xi(\xi^4+\xi_0^2)^3}. \tag{A13}$$

In the following, we will integrate $g_1$, $g_2$ and $g_3$ respectively. The integral of the rational algebraic fraction in the variable $g_1$ is found to be

$$\int \frac{3\xi^6\xi_0^3 + 5\xi^4\xi_0^3 - \xi^2\xi_0^5 + \xi_0^5}{\xi^2(\xi^4+\xi_0^2)^2}\,d\xi = -\frac{\xi_0}{\xi} + \frac{\xi^3\xi_0}{\xi^4+\xi_0^2} - \frac{\xi\xi_0^3}{\xi^4+\xi_0^2} = g_5. \tag{A14}$$

Therefore, $g_1$ can be integrated by parts. The result is

$$\int_{\xi_0}^{\infty} g_1\,d\xi = 2(1-\nu)\left\{g_5 \arctan\xi\Big|_{\xi_0}^{\infty} - \int_{\xi_0}^{\infty}\left[\frac{-\xi_0}{\xi(1+\xi^2)} + \frac{\xi^3\xi_0 - \xi\xi_0^3}{(\xi^4+\xi_0^2)(1+\xi^2)}\right]d\xi\right\}$$

$$= 2(1-\nu)\{\arctan\xi_0 + \tfrac{1}{4}[4\xi_0\ln\xi - \xi_0\ln(\xi^4+\xi_0^2)]_{\xi_0}^{\infty}\}$$

$$= 2(1-\nu)[\arctan\xi_0 - \tfrac{1}{2}\xi_0\ln\xi_0 + \tfrac{1}{4}\xi_0\ln(1+\xi_0^2)]. \tag{A15}$$

The variable $g_2$ can be expressed as partial fractions:

$$g_2 = \frac{\xi_0}{\xi} - \frac{\xi^3\xi_0}{\xi^4+\xi_0^2} + \frac{-\xi^3\xi_0^3 + 3\xi\xi_0^5}{(\xi^4+\xi_0^2)^2} + \frac{4\xi^4\xi_0^3 - 4\xi\xi_0^7}{(\xi^4+\xi_0^2)^3}. \tag{A16}$$

Then, the integration of eqn (A16) is straightforward:

$$\int_{\xi_0}^{\infty} g_2\,d\xi = \xi_0\ln\xi + \frac{\xi^4\xi_0^3 - \xi_0^5 - 2\xi^2\xi_0^5 - (\xi^6\xi_0 + 2\xi^4\xi_0^3 + \xi_0^5)\ln(\xi^4+\xi_0^2)}{4(\xi^4+\xi_0^2)^2}\Bigg|_{\xi_0}^{\infty}$$

$$= \frac{\xi_0}{4(1+\xi_0^2)} - \tfrac{1}{2}\xi_0\ln\xi_0 + \tfrac{1}{4}\xi_0\ln(1+\xi_0^2). \tag{A17}$$

The variable $g_3$ can also be expressed as the following partial fractions:

$$g_3 = \frac{(1-2\nu)\xi_0}{\xi} + \frac{(1-2\nu)(-\xi^3\xi_0 + 3\xi_0^3)}{\xi^4+\xi_0^2} + \frac{(-7+8\nu)\xi^3\xi_0^3 + 3\xi\xi_0^5 - 4(1-2\nu)\xi_0^4}{(\xi^4+\xi_0^2)^2} + \frac{4\xi^3\xi_0^5 - 4\xi\xi_0^7}{(\xi^4+\xi_0^2)^3}. \tag{A18}$$

By collecting the terms which have an even power of $\xi$ in the numerator, $g_3$ can be rearranged as

$$g_3 = \frac{(1-2\nu)\xi_0}{\xi} - \frac{(1-2\nu)\xi^3\xi_0}{\xi^4+\xi_0^2} + \frac{(-7+8\nu)\xi^3\xi_0^3 + 3\xi\xi_0^5}{(\xi^4+\xi_0^2)^2} + \frac{4\xi^3\xi_0^5 - 4\xi\xi_0^7}{(\xi^4+\xi_0^2)^3} + \frac{(1-2\nu)\xi_0^2(3\xi^4-\xi_0^2)}{(\xi^4+\xi_0^2)^2}. \tag{A19}$$

The integration is similar to (A17) except the last term. Observe that the last term can be integrated to be

$$\int \frac{(1-2\nu)\xi_0^2(3\xi^4-\xi_0^2)}{(\xi^4+\xi_0^2)^2}\,d\xi = -\frac{(1-2\nu)\xi_0^2\xi}{\xi^4+\xi_0^2}.$$

Carrying out the integration of the remaining parts of $g_3$, we have

$$\int_{\xi_0}^{\infty} g_3\,d\xi = (1-2\nu)\xi_0\ln\xi - \frac{(1-2\nu)\xi_0\ln(\xi^4+\xi_0^2)}{4} - \frac{(1-2\nu)\xi\xi_0^2}{\xi^4+\xi_0^2}$$

$$+ \frac{(7-8\nu)\xi^4\xi_0^3 + (5-8\nu)\xi_0^5 - 2\xi^2\xi_0^5}{4(\xi^4+\xi_0^2)^2}\Bigg|_{\xi_0}^{\infty},$$

$$= -\frac{(1-2\nu)\xi_0\ln\xi_0}{2} + \frac{(1-2\nu)\xi_0\ln(1+\xi_0^2)}{4} - \frac{\xi_0}{4(1+\xi_0^2)}. \tag{A20}$$

Combining eqns (A15), (A17) and (A20), the function $I_0$ is found to be

$$I_0(\xi_0) = \frac{2}{\pi}\arctan\xi_0 + \frac{(1-2\nu)}{2\pi(1-\nu)}\xi_0 \ln\frac{1+\xi_0^2}{\xi_0^2} - \frac{\xi_0}{2\pi(1-\nu)(1+\xi_0^2)}. \tag{A21}$$

*Function $I_1$*

From eqns (A3)–(A7), applying the same transformation $\xi = \sinh s$ as we do in eqn (A9) and denoting $\eta = z/a$, the dilation $\varepsilon_{kk} = u_{k,k}$ is simply

$$\varepsilon_{kk} = -\frac{2(1-2\nu_s)t_0}{\pi(1-\nu_s)a}\hat{G}_{,zz} = -\frac{2(1-2\nu_s)t_0}{\pi(1-\nu_s)a}\frac{\eta\xi}{\xi^4+\eta^2}. \tag{A22}$$

Substituting (A22) into (A2) leads to the closed-form expression for $I_1$

$$I_1 = \frac{4}{\pi}\int_0^{h/a}\int_0^{\infty}\frac{\eta^2\xi^2}{(\xi^4+\eta^2)^2}\left(\frac{r}{a}\right)\mathrm{d}\left(\frac{r}{a}\right)\mathrm{d}\left(\frac{z}{a}\right) = \int_0^{h/a}\int_{\eta}^{\infty}\frac{\eta^2}{\xi(\xi^4+\eta^2)}\,\mathrm{d}\xi\,\mathrm{d}\eta$$
$$= \frac{1}{\pi}\left(2\arctan\xi_0 + \xi_0\ln\frac{1+\xi_0^2}{\xi_0^2}\right), \tag{A23}$$

where $\xi_0 = h/a$.